ISSN 1063-7826, Semiconductors, 2014, Vol. 48, No. 4, pp. 476–480. © Pleiades Publishing, Ltd., 2014.
Original Russian Text © S.M. Pescherova, A.I. Nepomnyaschih, L.A. Pavlova, I.A. Eliseev, R.V. Presnyakov, 2014, published in Fizika i Tekhnika Poluprovodnikov, 2014, Vol. 48, No. 4, pp. 492–497.



# Morphological Characteristics of Grain Boundaries in Multicrystalline Silicon

**S. M. Pescherova^, A. I. Nepomnyaschih, L. A. Pavlova, I. A. Eliseev, and R. V. Presnyakov**

*Vinogradov Institute of Geochemistry, Russian Academy of Sciences, Siberian Branch, Irkutsk, 664033 Russia*

*^e-mail: spescherova@mail.ru*

Submitted March 28, 2013; accepted for publication September 20, 2013

**Abstract**—The structure of multicrystalline silicon and the distribution of the nonequlibrium charge-carrier lifetime over the surface and in the bulk of samples are investigated. Regular dependences of the electrical characteristics on the structure of grains and grain boundaries are established. Grain boundaries in multisilicon grown by the Bridgman–Stockbarger technique from a melt of metallurgical grade silicon are investigated. Metallographic and microscopic descriptions of grain boundaries can be used in fitting the crystallization conditions for growing multisilicon with the perfect structure for solar-power engineering.

**DOI:** 10.1134/S1063782614040228

## 1. INTRODUCTION

The distribution of electrical parameters in multicrystalline silicon (multisilicon, MS) ingots used as a material for solar cells is determined, first of all, by the structure of the MS [1]. Such factors as the existence of grain boundaries of different types in an ingot, grain size and parameters of the mutual orientation of grains, and density of microdefects and features of their interaction with impurities strongly affect one of the main electrical characteristics of MS, i.e. the nonequilibrium charge-carrier (NCC) lifetime $\tau$. The high sensitivity of this parameter to structural defects suggests that its distribution in the bulk of an ingot, which is typical of MS [2]. The aim of this study is to establish the main characteristics of the macrostructure of MS crystals. Studying the morphological features of grain boundaries is necessary for understanding MS macro- and microstructure formation upon directional crystallization by the Bridgman–Stockbarger technique. In addition, in the main focus of this study is recombination phenomena caused by MS macrostructure features.

## 2. EXPERIMENTAL

We investigated MS crystals with different impurity contents that depend on the initial material chosen for directional crystallization. In particular, a Krs 145 crystal was grown from the semiconductor silicon scrap and a Krs 26n crystal, from metallurgical grade silicon (ZAO Kremnii, Shelekhov, Irkutsk oblast).

To study the electrical activity of extended defects, we performed discrete measurements of the effective NCC lifetime in the bulk of MS ingots. The effective NCC lifetime was measured on a Taumetr-2M setup by the contactless microwave resonance method using the photoconductivity decay curve. Photocarriers were generated by pulsed laser irradiation of the investigated MS area with a wavelength of 1.06 μm. The effective NCC lifetime was measured by an MF1535 standard [3]. The level of the initial point on the decay curve was 0.7 of the photoconductivity signal and the level of the final point, $0.7/e$ of it. This allowed us to exclude the effect of higher modes and transient processes related to the switching of electronics, which are the drawback of this standard.

We recorded the effective NCC lifetimes corresponding to $2 \times 2$-mm sequential MS surface areas comparable with a light spot diameter of 2 mm.

The main criteria for separating the types of grain boundaries in MS were regularities of the variation in the NCC lifetime distribution in the bulk of MS and features of the defect-sensitive relief, which were revealed using a JXA8200 electron probe X-ray microanalyzer and an atomic force microscope after multistage metallographic etching. We recorded topographic features of the microrelief of the MS crystal surfaces treated in a selective etch. To study the morphological features, the MS samples were mechanically polished with diamond paste and then treated in a polishing etch (HF and $HNO_3$) for 2–3 min at room temperature. The duration of multistage layer-by-layer selective acid etching for 2 min with a Desha etch was chosen experimentally and, depending on the impurity contents in the MS samples, was 20 min for scrap MS and 2–4 min for MS from the metallurgical raw material [4]. The aim of etching was to form a defect-sensitive surface relief for further investigation and separation of grain boundary types in MS by electron probe X-ray microanalysis (EPMA) and atomic force microscopy (AFM).

General parameters of multicrystalline silicon

| Crystal | Resistivity, Ω cm | Charge carrier mobility, $cm^2/(V\,s)$ | Average charge-carrier lifetime, μs | Conductivity type |
|---|---|---|---|---|
| Krs 145 | 10 | 245 | 14.7 | *p* |
| Krs 26n | 0.05 | 150 | 2.4 | *p* |

## 3. RESULTS AND DISCUSSION

The electrical parameters of MS strongly depend on the degree of silicon purity and are structure-sensitive; therefore, in addition to the corresponding cleaning of silicon, it is necessary to pay special attention to the MS structure, forming it during directional crystallization such as to a large-grained column ingot grown with the minimum number of grain boundaries and the maximum homogeneous distribution of electrical characteristics.

The main electrical characteristics of the investigated MS ingots are given in the table. To study the effect of grain boundaries on the main electrical parameter of MS, i.e., the NCC lifetime, we used the contactless measuring method, which allowed us to follow the NCC lifetime variation depending on the presence of grain boundaries of different types in the investigated areas. The effective NCC lifetime directly depends on the surface texture and defects and is merely one of the components of the bulk NCC lifetime for a limited investigated crystal surface area. Upon movement of the Taumer-2M probe with a step of 2 mm the value of $\tau$ changes, which is related to the crystal structure and distribution of impurities in the bulk and on the surface of the investigated area. The measurements of $\tau$ were performed on the surfaces of the samples of an MS longitudinal length cut along the ingot growth axis. Figure 1 shows scanned images of surface fragments for the Krs 145 and Krs 26n samples with different microstructures corresponding to the NCC lifetimes measured in them.

The Krs 145 sample macrostructure (Fig. 1a) consists of even columns of large crystallites with continuous straight boundaries. Such a structure occupies over 80% of the ingot. The average NCC lifetime measured along the direction marked in Fig. 1a is 14.2 μs. It can be seen that sharp changes in $\tau$ are observed in areas 4 with $\tau_{min}$ = 8.8 μs and 10 with $\tau_{max}$ = 25 μs. It can be seen in the image of the Krs 145 crystal surface (Fig. 1a) that area 4 has no visible grain boundaries,

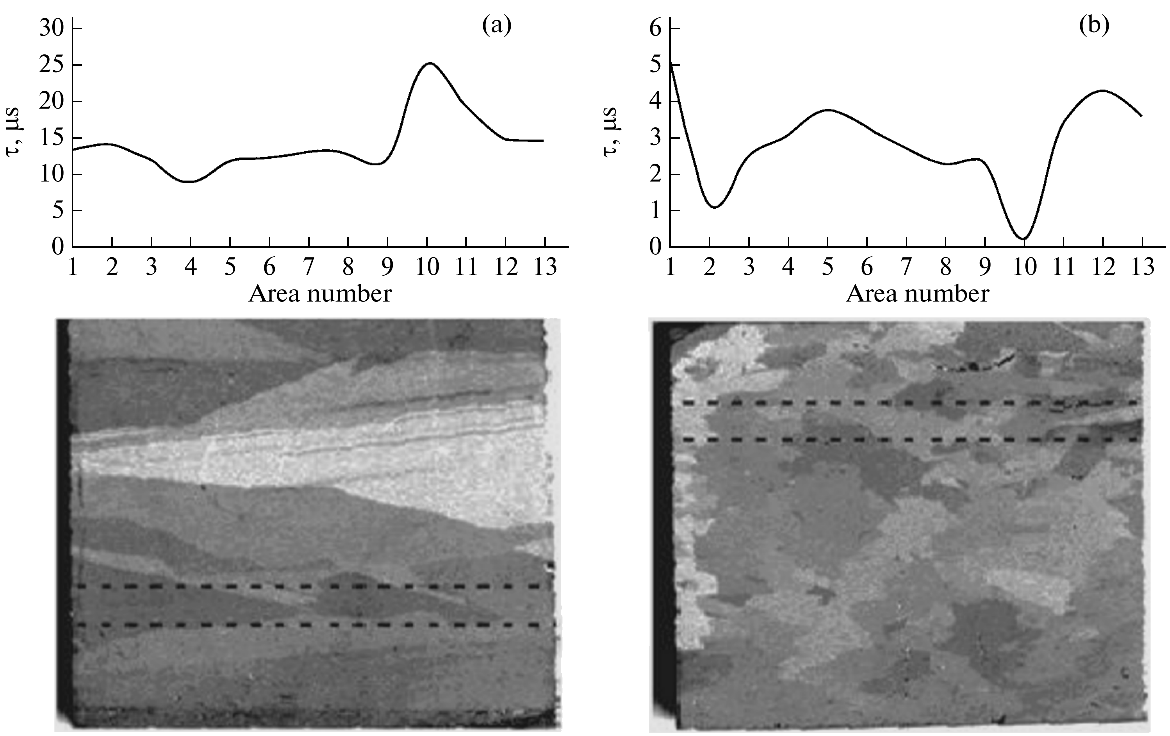


**Fig. 1.** NCC life time distribution in areas 1–13 shown by dashed lines in sample images in the ingot growth axis direction for (a) Krs 145 and (b) Krs 26n. Step-by-step measurement areas are 2 × 2 mm square, according to a measuring probe size of 2 × 2 mm and a step of 2 mm.

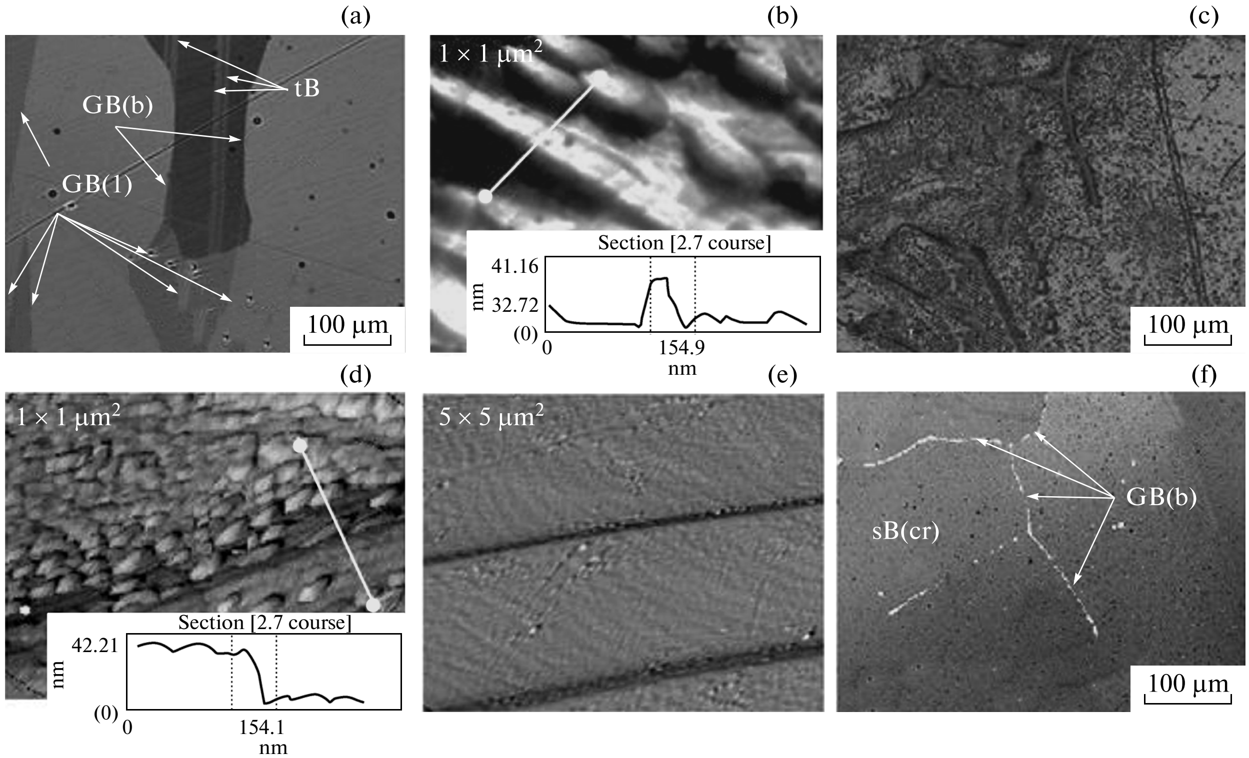


**Fig. 2.** Grain boundaries in multisilicon: (a, f) backscattered electron images of the Krs 145 and Krs 26n MS surfaces polished with diamond paste, (b, d, e) grain boundary AFM images at large magnification, and (c) backscattered electron image of surface *f* after etching.

since it belongs completely to a large crystallite; area 10, on the contrary, includes individual grains and, consequently, grain boundaries.

For the Krs 26n sample (Fig. 1b), the average value of $\tau$ is much smaller than that for the Krs 145 sample and amounts to 2.9 μs. In areas 10 and 12, the minimum ($\tau = 0.3$ μs) and maximum ($\tau_{max} = 4.3$ μs) NCC lifetimes were detected. As in the Krs 145 sample, the area with the minimum NCC lifetime contains a smaller number of visible grain boundaries on the sample macrostructure image: area 10 includes 3 grains and area 12, 5 grains (Fig. 1b).

The boundaries separating the neighboring grains and misoriented with respect to each other and to the plane parallel to the growth direction by an angle exceeding 5°–7° are considered to be general boundaries (GBs) [5]. Since the misorientation of neighboring crystallites on the surface treated with the 10% aqueous solution of KOH manifests itself as grey grain contrast, one can clearly see the GBs on the MS surface. In the image of the MS macrostructure (Figs. 1a and 1b), they can be seen as the boundaries between grey regions of different intensities. The boundaries in MS were studied in more detail by EPMA and AFM together with the use of selective acid etching techniques. The structural investigations allowed us to reveal the grain boundary types and their quantitative and morphological characteristics in the investigated areas of both crystals. The areas corresponding to the minimum NCC lifetime (4 and 10 in the Krs 145 and Krs 26n crystals, respectively) contain an enhanced number (no less than 4) of special subgrain boundaries (sBs). The number of GBs in these areas is no more than 2. Moreover, in the areas with the maximum NNC lifetime (10 and 13 in the Krs 145 and Krs 26n crystals, respectively) the presence of GBs does not significantly affect the measured quantity. These areas are characterized by the absence of crossing sBs (sBs(cr)). The distribution of the effective lifetime over the MS surface is undoubtedly related to the presence of grain boundaries in the investigated areas. Obviously, the effect of any boundary on NCC-lifetime degradation depends, first of all, on the type of boundary. The negative effect of GBs on $\tau$ is smaller than that of special boundaries. The structural features of general and special grain boundaries were investigated by EPMA and AFM. Two types of GBs were revealed: linearized and break boundaries. They are denoted in Figs. 2a and 2f as GB(l) and GB(b), respectively. Figures 2b and 2d present AFM images of these boundaries. In the images of polished MS surfaces (Figs. 2a and 2f), along with GBs, twin boundaries (tBs) are shown and an AFM image of this type of boundaries is presented (Fig. 2e).

Having estimated the contrast of neighboring crystallites separated by the linearized GB, one can see that neighboring crystallites are less misoriented with respect to each other than crystallites with a common break boundary. This phenomenon can be observed by a change in the image contrast of neighboring crystallites [6]. In the AFM image of GB(l) in Fig. 2b, one can see morphological differences between neighboring crystallites. On the surface of the crystallite shown below the boundary, nanosized globules are observed arranged mainly in a staggered order, while the surface of the upper crystallite consists of extended grooves arranged in the same way. The boundary line on the etched surface retains its linearity and the boundary regions are dissolved during etching, as can be seen in the AFM image obtained at a magnification of 3000 (Fig. 2b). The surface relief profile indicates that the surface of the upper crystallite has a pronounced relief related, most probably, to microdefects easily identified as etching wells. The feature of this boundary type is that areas with the strongest bonds are stable against acids, while the boundary areas of neighboring grains are etched stronger than the boundary. The surface relief along the line crossing the boundary in Fig. 2b indicates that both neighboring grains are equidistant from the boundary top by 40–50 nm. The boundary is asymmetrical in cross section and consists of two conjugated parts, each having a structure caused by the crystallographic features of an adjacent grain. Thus, if the bonds at the boundary are stronger than those in the boundary layer of the grain, then during etching the boundary line is dissolved slower than the neighboring parts of the grains. Therefore, the linearized GB has its own structure. In multisilicon from metallurgical grade silicon (Krs 26n, Fig. 2f), the grain boundaries of this type in the ingot cross section are almost always homogeneously (except for defect areas and dislocations) conjugated areas of neighboring crystallite structures forming a continuous boundary line (linearized GB). Microdefects at the boundaries revealed by etching (arbitrary etching wells) do not affect the shape and direction of the boundary itself. Most likely, they reveal areas of weak conjugation of the planes of neighboring grains the characteristic feature of which is various lattice disturbances. The enhanced microdefect concentration in the grain areas is characteristic, as a rule, of one of the two neighboring grains separated by the linearized GB. Grains separated by the linearized GBs (Figs. 2a and 2f) are of contrasting colors, i.e., misoriented with respect to each other. In both cases, the boundary lines retain their linearity up to the next triple boundary joint.

Another type of GB observed in MS is break GBs shown in Figs. 2e and 2f and in the AFM image (Fig. 2d). The direction of a boundary or its shift changes stepwise, which results in the formation of so-called facets of different sizes depending on the boundary shift. In many cases, the faceted GSs(b) can be accompanied by twin boundaries. Figure 2d presents a fragment of the GB(b) for the case of strong AFM magnification. The plane of the etched surface of the grain located below the boundary is lower than the upper grain by 42.2 nm; the boundary line in itself is a thin face between the etched planes of the neighboring grain surfaces. In the upper grain, one can see dense rows of dislocation lines along the boundary (in this case, it is reasonable to call the boundary the break line or break boundary), which confirms the obligatory participation of dislocations in the development of boundaries of this type. The stronger misorientation of the neighboring grains, the stronger the boundary is etched. Figures 2c and 2f show the Krs 26n MS surface before and after etching; in comparison with other boundaries on the surface after etching, break boundaries are the most etched. It means that these boundaries have the highest defect density among all boundaries. Indeed, in the backscattered electron image of the polished MS surface, one can see microinclusions (bright areas) localized along the GDs(b) [7]. During etching, microinclusions together with other possible microdefects form grooves and cracks on the sample surface (Fig. 2c).

There are twin boundaries of two types in MS: coherent and incoherent [8]. They can form associations of parallel coherent boundaries conjugated by incoherent ones. In this case, neighboring blocks are misoriented and the electrical properties of MS sharply degrade. In particular, in areas 5–9 and 11–13 on the NCC lifetime distribution curve for Krs 145 (Fig. 1a) and in areas 5–10 and 13 on the curve for Krs 26n (Fig. 1b) aggregates of twin boundaries are observed. After etching, twin boundaries look like even grooves with plane-parallel walls. Grain texture roughness remains invariable on both sides of the boundaries, especially in scrap MS, i.e. Krs 145 (Fig. 2e).

Along with GBs or grain boundaries separating areas with different crystallographic parameters, there are boundaries inside grains or so-called special boundaries with a misorientation angle of less than 5°. They are formed by the subsequent motion of dislocation planes (networks) within one grain that separate its parts into areas deviated by a small angle. The dislocation networks contracted in lines along the GBs(b) form special concomitant subgrain boundaries (sBs(co)), which exist in all MS samples. In scrap MS, they are met very rarely, while in MS from metallurgical silicon, in each sample. In Krs 26n, these boundaries contain impurity inclusions localized at dislocations (Fig. 3a). Special boundaries can not only be localized along the GBs(b) but also cross grain areas. As a rule, they represent etching wells arranged in series on dislocations and connected by the subgrain shift plane line at a small angle. The crossing subgrain boundaries connect the opposite grain sides and are effective sinks for impurities and defects. Special sBs(cr) appear when the GB(b) bending curvature cannot be compensated by twinning or facets; then, its start is determined by the step top and the finish, by the opposite boundary (Fig. 3b). Such boundaries can

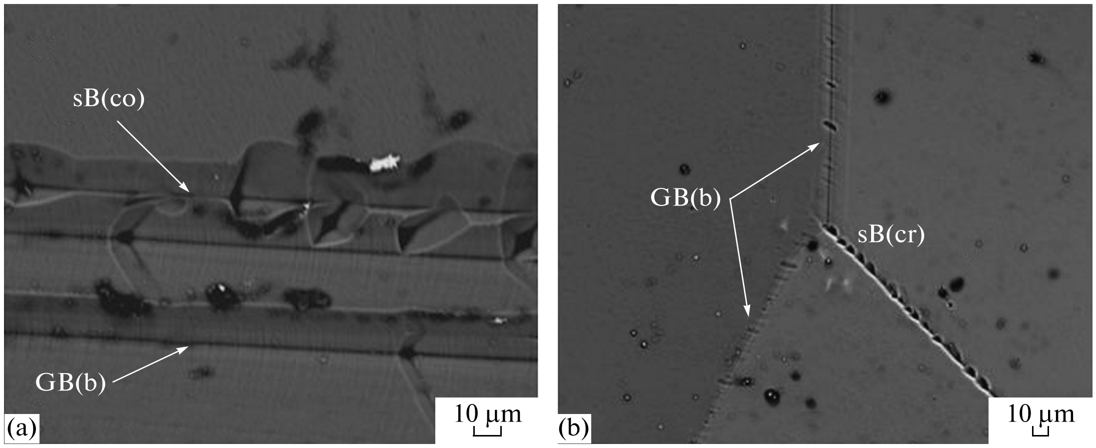


**Fig. 3.** Backscattered electron images of special grain boundaries on the surface of the longitudinal cut of Krs 26n MS: (a) sB(co) concomitant and (b) crossing boundary sB(cr).

be observed only after etching the MS surface, since they yield no image contrast on a polished and untreated surface. The possibilities of local EPMA in determining the chemical composition of the surface are restricted by limiting impurity concentrations; however, the sharp contrast of etching wells on sBs(cr), which is not related to the crystallographic parameters, makes us conclude that the crossing boundaries contain impurities in low concentrations [8]. Special crossing boundaries are geometrically required to compensate GB(b) bent contours in small grains or for the replacement of the GB in triple boundary joints for the case of broken linearity of grain sides or strong distortions of evenness of GB lines at bending points.

## 4. CONCLUSIONS

Upon multisilicon crystal growth from melt by the vertical Bridgman–Stockbarger technique, several types of grain boundaries form. Depending on the mutual orientation of grains that form the boundary and the degree of misorientaiton of these grains with respect to the plane perpendicular to the growth direction, grain boundaries of different types are formed. There are general and special boundaries. The general boundaries can be observed directly on the cut surface of MS ingots, since they separate misoriented grains of different colors. The main types of general boundaries are linearized boundaries separating grains oriented along the growth axis and break boundaries forming between grains deviated from the growth direction. Thus, the disturbance of the directionality of crystallites along the ingot growth axis during crystallization leads to the formation and growth of crystallites separated by general break boundaries. In addition, it was established that the break boundaries demonstrate higher recombination activity as compared with linearized boundaries. Moreover, they represent areas with high concentrations of such defects as twin boundaries, dislocation networks, special boundaries, and microinclusions. Special boundaries and other microdefects are observed at the bending points of break boundaries and are effective sinks for impurities, which strongly affects the distribution of the electrical properties in the bulk of an ingot. Thus, for the case of growing MS crystals by the Bridgman–Stockbarger technique, certain crystallization conditions should be satisfied at which large crystallites, mainly with linearized general boundaries, can be directed vertically. In addition, it is important to control impurity contents in the initial melt which are responsible for the occurrence of microinclusions and their distribution over the grain boundaries in MS.

## REFERENCES

1. B. A. Krasin, A. I. Nepomnyashchikh, A. S. Tokarev, T. S. Shamirzaev, R. V. Presnyakov, and A. P. Maksikov, Izv. Vyssh. Uchebn. Zaved., Mater. Elektron. Tekh., No. 1, 28 (2005).
2. B. A. Krasin, A. I. Nepomnyashchikh, Yu. S. Mukhachev, and R. V. Presnyakov, Izv. Vyssh. Uchebn. Zaved., Mater. Elektron. Tekh., No. 1, 73 (2006).
3. www.igc.irk.ru/CKP/spisok-ckp19.html
4. R. Einhaus, E. Vazsonyi, J. Szlufcik, and J. Nijs, Sol. Energy Mater. Solar Cells **74**, 155 (2002).
5. E. V. Naidenkin, N. V. Girsova, M. B. Ivanov, and V. N. Danilenko, Fiz. Mezomekh. **7** (S2), 42 (2004).
6. L. A. Pavlova, A. I. Nepomnyashchikh, and S. M. Peshcherova, J. Surf. Invest.: X-ray, Synchrotron Neutron Tech. **5**, 949 (2011).
7. W. Seifert, G. Morgenstern, and M. Kittler, Semicond. Sci. Technol. **8**, 1687 (1993).
8. S. M. Peshcherova, L. A. Pavlova, A. I. Nepomnyashchikh, I. A. Eliseev, and Yu. V. Sokol'nikova, Izv. Vyssh. Uchebn. Zaved., Mater. Elektron. Tekh., No. 4, 12 (2012).

*Translated by E. Bondareva*